

Pattern formation of dipolar colloids in rotating fields: Layering and synchronization.[†]

Sebastian Jäger^a and Sabine H. L. Klapp^{*a}

Received Xth XXXXXXXXXXXX 20XX, Accepted Xth XXXXXXXXXXXX 20XX

First published on the web Xth XXXXXXXXXXXX 200X

DOI: 10.1039/b000000x

We report Brownian dynamics (BD) simulation and theoretical results for a system of spherical colloidal particles with permanent dipole moments in a rotating magnetic field. Performing simulations at a fixed packing fraction and dipole coupling parameter, we construct a full non-equilibrium phase diagram as function of the driving frequency (ω_0) and field strength (B_0). This diagram contains both synchronized states, where the individual particles follow the field with (on average) constant phase difference, and asynchronous states. The synchronization is accompanied by layer formation, *i.e.* by spatial symmetry-breaking, similar to systems of induced dipoles in rotating fields. In the permanent-dipole case, however, too large ω_0 yield a breakdown of layering, supplemented by complex changes of the single-particle rotational dynamics from synchronous to asynchronous behavior. We show that the limit frequencies ω_c can be well described as a bifurcation in the nonlinear equation of motion of a single particle rotating in a viscous medium. Finally, we present a simple density functional theory, which describes the emergence of layers in perfectly synchronized states as an equilibrium phase transition.

1 Introduction

The dynamics of anisotropic particles driven by time-dependent, magnetic or electric, external fields is currently a topic receiving much attention. Many experimental and theoretical studies in this area focus on the field-induced dynamics of a *isolated* nanoparticle such as a magnetic rod,^{1–3} a magnetic chain⁴ or filament,⁵ or an optically excitable nanorod⁶ in a viscous medium. Understanding the resulting single-particle rotational dynamics is particularly important for actuators,² molecular switches, particles in optical traps,⁶ and in the more general context of microfluidics.³ From the theoretical side, these problems are often successfully analyzed on the basis of single-particle, nonlinear equations for the driven rotational motion in the presence of solvent-induced friction.^{1–3,6} Typically, the particle dynamics exhibits a “linear” regime at low driving frequencies, where the particle axis follows the field, and various types of nonlinear behavior at high frequencies, such as rotation against the torque.⁶ Many of these nonlinear phenomena, including transient behavior such as conformational transitions⁴ of magnetic chains following a sudden switch-on of the driving field, can also be observed experimentally.^{1,3}

Apart from the single-particle dynamics, another current focus concerns the *self-assembly* behavior in colloidal many-particle systems that are exposed to rotating fields. Indeed, in material science, time-dependent fields are currently realized as a powerful tool to control self-assembly processes, which

are an important prerequisite for synthesizing functional materials.^{7,8} A classical example in this context, first discussed by Martin *et al.*,⁹ are systems of paramagnetic (or polarizable) spherical particles in magnetic (electric) fields rotating in a plane. For sufficient field strength, both experiment and computer simulations^{9–11} reveal the formation of layers in the field plane, *i.e.* a *spatial* symmetry breaking induced by the rotating field. Indeed, a rotating in-plane field generates, on averaging over time, an inverted dipolar pair interaction with in-plane attraction and repulsion along the rotation axis.^{11,12} Therefore, the structures induced by planar rotating fields are markedly different from those observed in a constant and homogeneous field, which supports the formation of field-aligned chains (low densities)^{13–15} and bulk crystals.^{16,17}

The general idea to use time-dependent fields to tune pair interactions and thereby control the morphology of self-assembled structures has meanwhile become more and more popular (see Refs. 18,19), a recent example being the formation of self-healing membranes of superparamagnetic particles in tilted rotating fields.²⁰ Interestingly, these self-assembly phenomena can often be explained from an equilibrium perspective involving the free energy and resulting phase behavior of a many-particle system in a time-averaged field. Clearly, the crucial assumption in adopting this perspective, which is also often exploited in computer simulation studies (see *e.g.* Refs. 9,21) is that the particles follow the field *synchronously*.

In the present paper we explore, for a magnetic many-particle system, the *link* between the collective, self-assembly behavior, on the one hand, and the single-particle dynam-

^a Institute of Theoretical Physics, Technical University Berlin, Hardenbergstr. 36, 10623 Berlin, Germany. E-mail: klapp@physik.tu-berlin.de

ics, on the other hand. Specifically, we consider a ferrofluid subjected to a rotating in-plane field, where the ferrofluid is modeled by a system of dipolar soft spheres (DSS). The same model has been considered earlier in a computer simulation study by Murashov and Patey,²² where the aim was to demonstrate that layering occurs not only in systems of (super-)paramagnetic or polarizable particles (as those considered by Martin *et al.*^{9,10}), but also for particles with permanent dipoles. Here we investigate the driven DSS system both by Brownian dynamics (BD) computer simulations, which are described in Sec. 2, and by theory. As a first main result, we present in Sec. 3.2 a full non-equilibrium “phase” diagram indicating the domain of layer formation in the plane spanned by the frequency and strength of the driving field at constant equilibrium thermodynamic parameters. Secondly, to identify the role of mutual synchronization of the particles, we investigate in Sec. 3.3 the rotational dynamics within layered and unlayered states by analyzing suitable distribution functions. A similar strategy has recently been proposed in a dynamic density functional study of rod-like particles in rotating fields.²³ In Sec. 3.3.1 we show that the breakdown of layering observed at high frequencies in the ferrofluid system can be described by a single-particle theory similar to those used for field-driven single nanoparticles in viscous media.⁶ Finally, in Sec. 3.4, we propose a simple equilibrium density functional approach to investigate the role of *translational* entropy for layering in synchronized ferrofluid systems. The results are in good agreement with corresponding BD simulations. We close the paper with a brief summary and conclusions (Sec. 4).

2 Model and simulation methods

In our simulations we model the colloidal suspension by a system of dipolar soft spheres (DSS). The solvent is not explicitly taken into account. The DSS pair potential between two spheres is comprised of a repulsive potential U^{rep} and a point dipole-dipole interaction potential

$$U^{\text{DSS}}(\mathbf{r}_{ij}, \boldsymbol{\mu}_i, \boldsymbol{\mu}_j) = U^{\text{rep}}(r_{ij}) - \frac{3(\mathbf{r}_{ij} \cdot \boldsymbol{\mu}_i)(\mathbf{r}_{ij} \cdot \boldsymbol{\mu}_j)}{r_{ij}^5} + \frac{\boldsymbol{\mu}_i \cdot \boldsymbol{\mu}_j}{r_{ij}^3}. \quad (1)$$

In eqn (1), \mathbf{r}_{ij} is the vector between the positions of the particles i and j , r_{ij} its absolute value, and $\boldsymbol{\mu}_i$ is the dipole moment of the i th particle. The potential U^{rep} is the shifted soft sphere potential, which is given by

$$U^{\text{rep}}(r) = U^{\text{SS}}(r) - U^{\text{SS}}(r_c) + (r_c - r) \frac{dU^{\text{SS}}}{dr}(r_c), \quad (2)$$

where

$$U^{\text{SS}}(r) = 4\epsilon \left(\frac{\sigma}{r_{ij}} \right)^{12} \quad (3)$$

is the unshifted soft sphere (SS) potential for particles of radius σ . Further, $r_c = 2.5\sigma$ is the radius at which we cut off the potential U^{rep} .

We investigate the system using non-overdamped Brownian dynamics (BD) simulations (sometimes called Langevin dynamics simulations). The corresponding equations of motion for particles of mass m and moment of inertia I are²²

$$m\ddot{\mathbf{r}}_i = \mathbf{F}_i^{\text{DSS}} - \xi_T \dot{\mathbf{r}}_i + \mathbf{F}_i^G \quad (4)$$

$$I\dot{\boldsymbol{\omega}}_i = \mathbf{T}_i^{\text{DSS}\perp} + \mathbf{T}_i^{\text{ext}\perp} - \xi_R \boldsymbol{\omega}_i + \mathbf{T}_i^{\text{G}\perp}. \quad (5)$$

In these equations $\xi_T = k_B T/D$ and $\xi_R = k_B T/D_r$ are friction coefficients with k_B and T being Boltzmann’s constant and temperature, respectively, while D and D_r are the translational and rotational diffusion constants. Furthermore $\boldsymbol{\omega}_i$ is the angular velocity of particle i , \mathbf{F}_i^G and \mathbf{T}_i^G are random Gaussian forces and torques, $\mathbf{T}_i^{\text{ext}}$ are torques due to an external field, and $\mathbf{T}_i^\perp = \mathbf{T}_i - (\boldsymbol{\mu}_i \cdot \mathbf{T}_i) \boldsymbol{\mu}_i / \mu_i^2$. Their cartesian components ($\alpha, \beta = x, y, z$) satisfy

$$\langle F_{i\alpha}^G(t) \rangle = 0 \quad (6)$$

$$\langle T_{i\beta}^G(t) \rangle = 0 \quad (7)$$

as well as

$$\langle F_{i\alpha}^G(t) F_{j\beta}^G(t') \rangle = 6k_B T \xi_T \delta_{ij} \delta_{\alpha\beta} \delta(t - t') \quad (8)$$

$$\langle T_{i\alpha}^G(t) T_{j\beta}^G(t') \rangle = 6k_B T \xi_R \delta_{ij} \delta_{\alpha\beta} \delta(t - t'). \quad (9)$$

As eqns (6)-(9) show, the friction coefficients and the probability distributions of the random forces and torques are related via the fluctuation-dissipation theorem. This ensures that the system approaches a canonical distribution of states characterized by a constant temperature T in the absence of an external drive. To deal with the long-ranged dipolar interactions, we used the Ewald summation method with conducting boundaries.²⁴ We have parallelized the evaluation of the Ewald sum in our simulation with OpenMP and MPI. The equations of motion were integrated with a Leapfrog algorithm.²⁵

The external field that the particles interact with rotates with frequency ω_0 in the $x - y$ -plane and is given by

$$\mathbf{B}(t) = B_0(\mathbf{e}_x \cos \omega_0 t + \mathbf{e}_y \sin \omega_0 t). \quad (10)$$

For convenience, we make use of the following reduced units: Field strength $B_0^* = (\sigma^3/\epsilon)^{1/2} B_0$; angular frequency $\omega_0^* = (m\sigma^2/\epsilon)^{1/2} \omega_0$; density $\rho^* = \sigma^3 \rho$; dipole moment $\mu^* = (\epsilon\sigma^3)^{-1/2} \mu$; and moment of inertia $I^* = (m\sigma^2)^{-1} I$. Unless stated otherwise, the simulations were carried out with 864 particles at density $\rho^* = 0.1$, dipole moment $\mu^* = 3$, moment of inertia $I^* = 0.025$, and temperature $T^* = k_B T/\epsilon = 1.35$. To verify our results, we also ran simulations with

up to 4000 particles. The translational and rotational diffusion constant were chosen to be $D = 0.1 \cdot (\epsilon\sigma^2/m)^{1/2}$ and $D_r = 3 \cdot (m\sigma^2/\epsilon)^{-1/2}$, respectively, and we used a timestep of $\Delta t = 0.0025 \cdot (m\sigma^2/\epsilon)^{1/2}$. These values are consistent with those chosen in earlier BD studies of rotating dipolar systems.²² We note, however, that the effects reported in the present paper also appear for other values of D and D_r .

3 Results and discussion

3.1 Zero field system

The zero field system, which represents our starting point, is characterized by a large dipolar coupling strength $\lambda = \mu^2/(k_B T \sigma^3) \approx 6.7$ and a relatively low density. As expected for such a strongly coupled system, the particles self-assemble into chainlike structures.^{15,26} This can be seen in the snapshot depicted in Fig. 1a. Our reason for considering a system of a coupling strength this high is that this seems to be a prerequisite for layer formation. Indeed, irrespective of the field strength, we did not observe any layering for values of λ that are smaller than approximately 4.6 (at the temperature $T^* = 1.35$).

Contrary to λ , our choice of the density is less restricted, since the layering phenomenon persists over a wide range of densities (at least up to $\rho^* = 0.4$). However, choosing the small density of $\rho^* = 0.1$ has the advantage that layers are easily discernible.

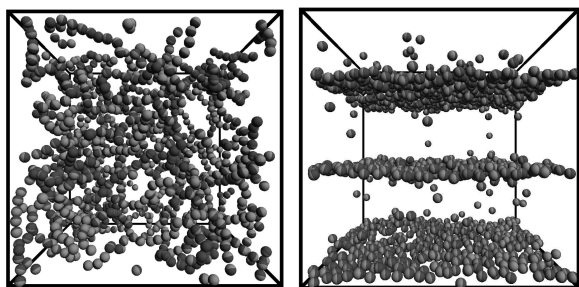


Fig. 1 (a) Snapshot of the system in zero field at $\rho^* = 0.1$, $T^* = 1.35$, and $\mu^* = 3$. (b) Snapshot of a system in a layered state. The strength and frequency of the field are $B_0^* = 12$ and $\omega_0^* = 15$, respectively.

3.2 The layering effect

We now consider the same system in rotating fields of various strengths B_0^* and frequencies ω_0^* . For sufficiently large B_0^* and not too high frequencies (see below), the particles arrange themselves into layers. An example of this is shown in Fig. 1b.

This phenomenon was first explained by Halsey, Anderson, and Martin.¹² They realized that the time-averaged potential between two particles i and j that rotate with the same angular frequency (given by the external field) and are aligned with each other, *i.e.* rotate circularly in a synchronized fashion with

$$\boldsymbol{\mu}_i(t) = \boldsymbol{\mu}_j(t) = \mu(\mathbf{e}_x \cos \omega_0 t + \mathbf{e}_y \sin \omega_0 t), \quad (11)$$

is given by

$$U^{\text{ID}}(\mathbf{r}_{ij}) = \tau^{-1} \int_{t_0}^{t_0+\tau} U^{\text{D}}(\mathbf{r}_{ij}, \boldsymbol{\mu}_i(t), \boldsymbol{\mu}_j(t)) dt = -\mu^2 \frac{(1 - 3 \cos^2 \Theta_{ij})}{2r_{ij}^3}. \quad (12)$$

In this equation, U^{D} is the dipole-dipole potential (see eqn (1)), $\tau = 2\pi/\omega_0$ is the oscillation period, and Θ_{ij} is the angle between the interparticle vector \mathbf{r}_{ij} and the direction perpendicular to the plane of the field. As shown by the last line in eqn (12), the time-averaged potential corresponds to an inverted dipolar (ID) potential, which is attractive if the angle Θ_{ij} satisfies $\cos^2 \Theta_{ij} < 1/3$, *i.e.* if the particles i and j are approximately in the same plane with respect to the field. Conversely, if the angle Θ_{ij} satisfies $1/3 < \cos^2 \Theta_{ij}$, the particles repel each other. This direction dependence of the ID potential explains why layers are a favorable configuration for a driven system in which the particles rotate synchronously.

Note that for the above argument to hold, the translational motion of the particles should be small compared to their rotational motion. More precisely, during one rotational period they should migrate much less than their own diameter.¹²

In the following we aim to determine more precisely the range of frequencies and field strengths at which layering occurs. To do that, we need a suitably defined order parameter. We tested several ones and compared them with one another. The order parameter that we will use here is given by

$$\psi = \frac{1}{N} \sum_{i=1}^N \langle n_i \rangle, \quad (13)$$

where N is the total number of particles, $\langle \dots \rangle$ denotes a time-average, and n_i is defined as follows: Consider a sphere of radius r_0 around particle i . Divide that sphere into two parts, one of which is given by the points within the sphere whose distance vector to particle i together with the z -axis encloses an angle Θ satisfying $-0.5 < \cos \Theta < 0.5$ (see Fig. 2). If there are more (less) particles in this equatorial volume than in the polar volume around particle i , set $n_i = 1$ (-1); if there are the same number of particles, set $n_i = 0$. Note that the radius r_0 was set to 8σ . Smaller as well as larger radii r_0 decrease the performance of the order parameter as we found by comparing the order parameter with the actual order observed in the system.

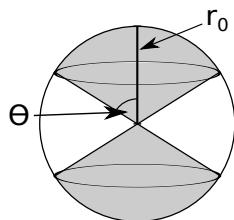


Fig. 2 Sketch of the polar and equatorial regions used in the definition of the order parameter.

Representative examples for the behavior of the resulting order parameter at constant angular frequency but increasing field strength are given in Fig. 3. As can be seen, in all the cases the value of ψ grows with the field strength until it almost reaches a value of 1. Since the layers are usually not perfectly defined in our Brownian dynamics simulations, the order parameter typically takes on values that are slightly smaller than 1 even at very high field strengths.

One also finds from Fig. 3 that there is a qualitative difference in the behavior of ψ at high and low frequencies: The order parameter grows much more steeply at large frequencies, which means that the layers do not slowly emerge upon increasing the field strength but appear very rapidly.

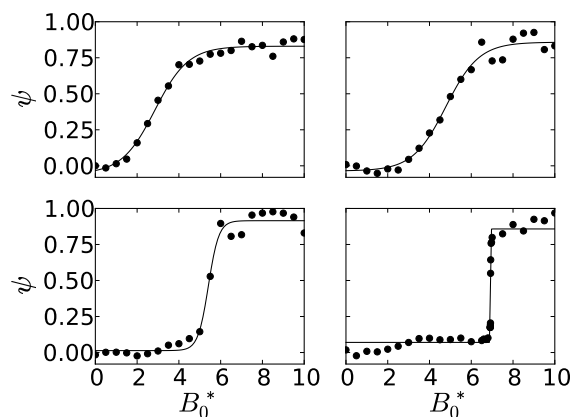


Fig. 3 The order parameter ψ at constant angular frequency (a) $\omega_0^* = 1$, (b) 20, (c) 30, (d) 40.

By inspecting snapshots corresponding to a given value of the order parameter, it turned out that the value $\psi_0 \approx 0.6$ may serve as an (approximate) lower limit for layer formation.

Based on that criterion, we have scanned a broad range of frequencies and field strengths for the occurrence of layers. The results of this exploration of the parameter space are summarized in Fig. 4. Note that every simulation was started from a random configuration to avoid hysteresis-like effects.

Within the layered “state”, the translational structure of one

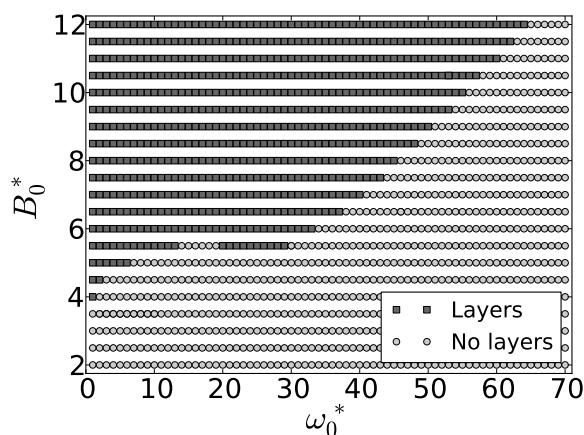


Fig. 4 Occurrence of layers depending on field strength and frequency of the driving field. The system parameters are chosen as described in Sec. 2.

layer is disordered and becomes more and more homogeneous with larger ω_0^* . In particular there is no pronounced hexagonal order as observed in earlier studies,⁹ even though the particles tend to have six nearest neighbors at high ω_0 . This absence of pronounced in-plane order is probably a consequence of the low density considered ($\rho^* = 0.1$) and the Brownian random forces. Furthermore, depending on the initial conditions, we typically observe two or three layers in our simulation box ($N = 864$), which corresponds to an average vertical distance between the layers of about seven to ten particle diameters.

The figure shows that the $\omega_0^* - B_0^*$ diagram is separated into a layered and a non-layered region. Upon increasing the frequency from zero, the boundary first remains at roughly constant field strength, until it begins to rise with the frequency. This behavior is mirrored in Fig. 3. The larger the frequency, the higher the field strength at which the order parameter attains large values.

A similar picture emerges from Fig. 5, where we have plotted the normalized absolute value of the magnetization, *i.e.* $M/M_0 = \langle |\mathbf{M}(t)| \rangle / M_0$ with $\mathbf{M}(t) = \sum_{i=1}^N \boldsymbol{\mu}_i(t)$ and $M_0 = N\mu$, as a function of B_0^* for several frequencies. Note that $|\mathbf{M}(t)|$ is essentially independent of time for the states considered in Fig. 5. Clearly, the magnetization behaves differently in the regimes of small and large frequencies. One also finds from Fig. 5 that a degree of magnetization of more than 80 percent is required for layer formation to occur.

In the following subsections, we will discuss the emergence and breakdown of layering in the different frequency regimes in more detail. Before doing so, it is worth to briefly comment on a technical issue encountered in our exploration of the parameter space (see Fig. 4) that concerns the behavior of the rotational temperature $T_{\text{rot}} = 1/(2(N-1)) \sum_{i=1}^N I\omega_i^2$. Upon

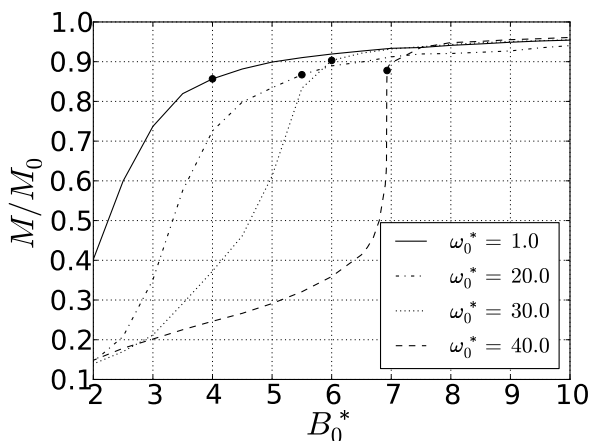


Fig. 5 Absolute value of the magnetization normalized with respect to its saturation value over field strength at different rotational frequencies. The dots indicate after which point the system is considered layered according to our order parameter.

increasing the driving frequency ω_0^* from zero (at fixed B_0^*), we typically also find T_{rot} to increase, while its translational counterpart $T_{\text{trans}} = 1/(3(N-1)) \sum_{i=1}^N m v_i^2$ stays approximately constant (close to the input value T). Similar temperature drifts have been observed in other non-equilibrium systems such as fluids in shear flow. In the latter context, the temperature is often redefined with respect to the differences between the actual velocity of the particle and that of the flow field.²⁷ Using a similar definition here (involving the difference between ω_i and ω_0), we find that this temperature is still not equal to T , but remains essentially constant over a broad range of frequencies. We also note that both the temperature drift and the actual location of the layer boundary in the $\omega_0^* - B_0^*$ diagram depend on the chosen value of the rotational friction constant.

3.3 Rotational dynamics in the layered state

As mentioned earlier, the key argument for the appearance of the layers is that the time-averaged interaction between two *fully synchronized* rotating dipoles favors an in-plane configuration. In the following, we will investigate in more detail to what extent this assumption is actually fulfilled within the layered region indicated in Fig. 4. To this end, we consider the distribution f of the phase differences ϕ_i between the dipolar vector of particle i in the $x - y$ -plane and the external field.

More precisely, we define f as

$$f(\phi) = \frac{1}{N\Delta\phi} \left\langle \sum_{i=1}^N \Theta(\phi_i - n\Delta\phi) - \Theta(\phi_i - (n+1)\Delta\phi) \right\rangle, \quad (14)$$

where Θ is the Heaviside function, $\Delta\phi$ is the interval length to which we want to resolve the distribution, n is a positive integer or zero that satisfies $n\Delta\phi \leq \phi < (n+1)\Delta\phi$, and, as before, $\langle \dots \rangle$ denotes a time-average.

We start by considering systems that are driven by fields of considerable strength ($B_0^* = 10$) with frequencies that admit layer formation (*cf.* Fig. 4). Results for the distribution f at three such frequencies ω_0^* are given in Fig. 6. For each value of ω_0^* one observes a single, pronounced peak, reflecting a synchronized “state”, in which the particles follow the field at constant phase difference. Note that the larger ω_0^* , the larger

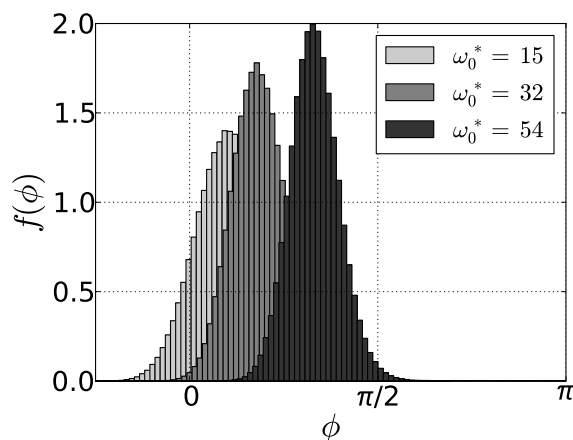


Fig. 6 Distribution of the phase differences at $B_0^* = 10$ and three frequencies ω_0^* with $\Delta\phi = \pi/48$. The systems are in layered states (see Fig. 4).

the phase difference between the particles and the field. This is not too surprising since an increase in the driving frequency implies an increase in the rotational friction due to the (implicit) solvent and the presence of neighboring particles. Further note that even though eqn (14) contains a time-average, the phase distributions of these layered systems are essentially independent of time.

To investigate the degree to which the particles actually rotate in the plane of the field, we also consider the distribution of the z -components of the angular frequencies

$$g(\omega_z^*) = \frac{1}{N\Delta\omega} \left\langle \sum_{i=1}^N \Theta(\omega_{i,z}^* - n\Delta\omega) - \Theta(\omega_{i,z}^* - (n+1)\Delta\omega) \right\rangle.$$

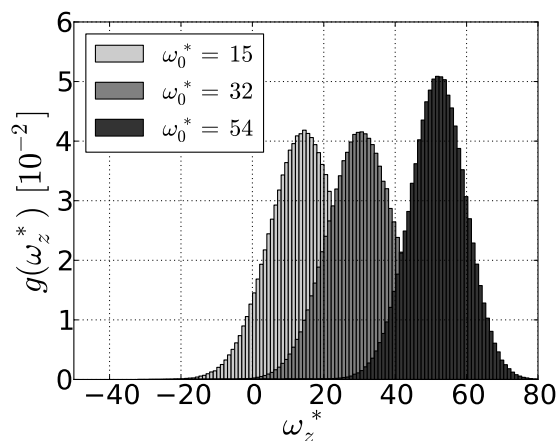


Fig. 7 Distributions of the z -component of the angular frequencies. Parameters are as in Fig. 6. The interval $\Delta\omega$ is set to 1.

In an ideal situation, in which the dipoles rotate perfectly with the field, the distribution g would have a single, sharp peak at $\omega_z^* = \omega_0^*$. Simulation results for g in the true many-particle system are shown in Fig. 7, where we have picked out the “states” already considered in Fig. 6. As expected in the layered regime, the functions g are characterized by one central peak around $\omega_z^* \approx \omega_0^*$. However, we also see that there is a significant broadness in the distribution (as there is in the corresponding peaks of f).

Finally, above a certain frequency, the layers disappear. This is reflected in the emergence of a double-peaked structure in the distribution of the phase differences, as illustrated in Fig. 8a. Moreover, we found that the non-averaged distribution of the phase differences is not independent of the time anymore. However, since we could not identify any *systematic* time-dependence in this regime, we restrict ourselves to considering the averaged distribution. The first peak in f at $\phi \approx \pi/4$ is due to particles that can still temporarily follow the field, whereas particles that are not able to do so anymore cause the structure of the rest of the distribution. The breakdown of layering is also visible in the distribution g . Contrary to what is seen in a layered system, the angular frequencies of the majority of the particles are distributed around $\omega_z^* \approx 0$ as shown in Fig. 8b. The much smaller peak at approximately the frequency of the external drive shows that only a small fraction of the particles follow the field at any given time. This fraction is further decreased as the frequency ω_0^* of the driving field increases. Typical distributions f and g at values of ω_0^* outside the layered regime are shown in Figs. 9a and 9b, respectively. Note that the roughly symmetric distribution of ω_z^* around approximately zero in Fig. 9b indicates that the particles are as likely to rotate in the direction of the field as they are to rotate in the opposite direction.

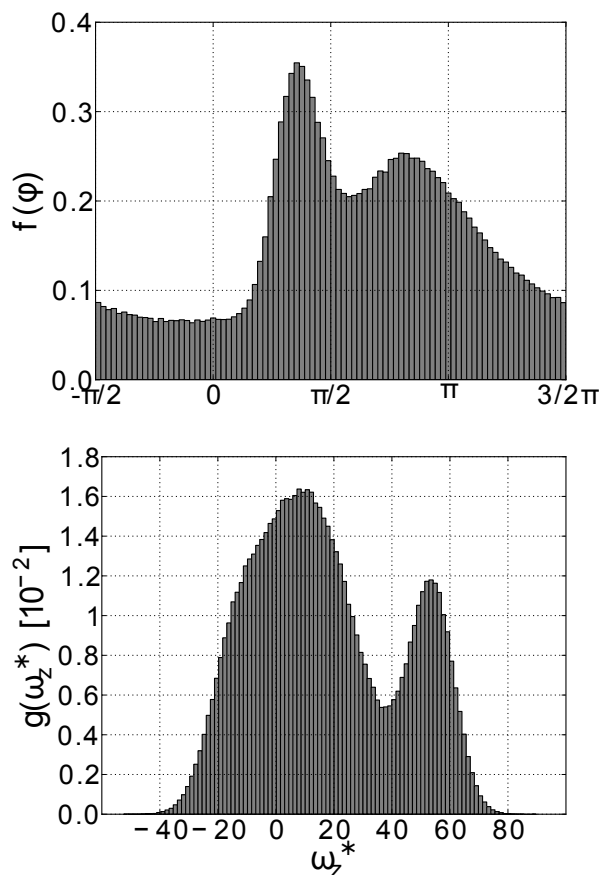


Fig. 8 (a) Distribution of the phase differences of the system at $B_0^* = 10$ and $\omega_0^* = 55.8$, *i.e.* just outside of the region of layer formation. The resolution is $\Delta\phi = \pi/40$. (b) Distribution of ω_z^* for a system at $B_0^* = 10$ and $\omega_0^* = 55.8$ with $\Delta\omega = 1$.

Further note that at the large values of B_0^* considered in this section, the transition between states with the particles following the field at fixed phase difference and states where this is not true anymore happens in a very small range of frequencies.

3.3.1 Effective single-particle theory. To understand the character of the high-frequency boundary between layered and non-layered states in more detail, we now aim to construct an effective theory that describes a single dipolar particle rotating in a viscous medium. A similar consideration has been suggested for optically torqued nanorods by Shelton *et al.*⁶ Clearly, such a single-particle approach cannot grant us direct insight into the formation of layers. However, it may help us to improve our understanding of the rotational dynamics isolated from many-particle effects. For simplicity, we assume that the rotational motion of the particle is restricted to the plane of the field and that it experiences rotational friction with fric-

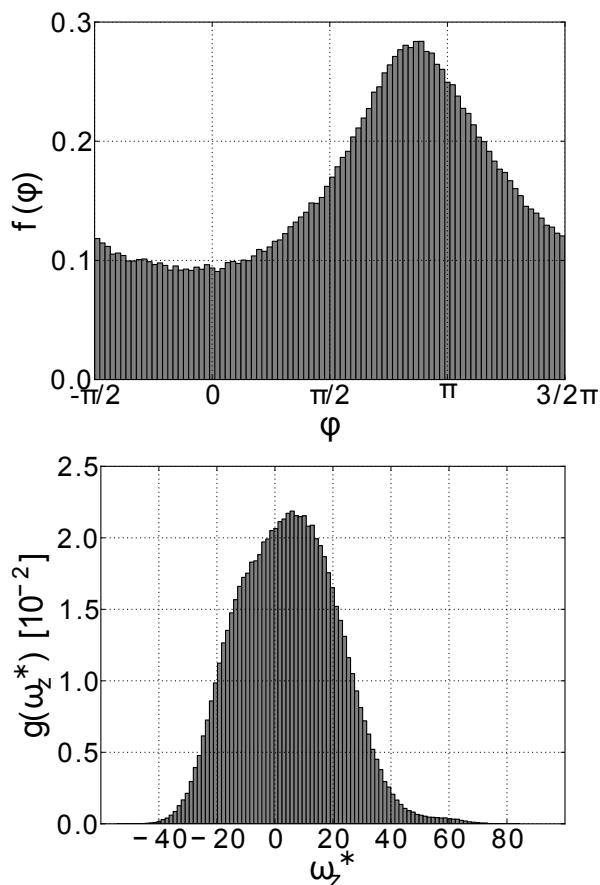


Fig. 9 (a) Distribution of phase differences of the system at $B_0^* = 10$ and $\omega_0^* = 60$. The system is unlayered. (b) Distribution of ω_z^* of the system at $B_0^* = 10$ and $\omega_0^* = 60$. The system is unlayered.

tion constant γ . Then the rotational equation of motion is

$$I\ddot{\alpha} = -\gamma\dot{\alpha} + \mu B_0 \sin(\omega_0 t - \alpha), \quad (15)$$

where α is the angle between the dipolar orientation and an arbitrary axis within the plane of the field. Equation (15) can be rewritten in terms of the phase difference $\phi = \omega_0 t - \alpha$ as

$$I\ddot{\phi} + \gamma\dot{\phi} = \gamma\omega_0 - \mu B_0 \sin \phi. \quad (16)$$

We first consider the simplified case of negligible moments of inertia, *i.e.* an overdamped situation. Then eqn (16) reduces to the first order equation

$$\frac{d\phi}{d\tau} = \frac{\omega_0}{\omega_c} - \sin \phi, \quad (17)$$

where $\omega_c = \mu B_0 / \gamma$ and $\tau = \omega_c t$. This nonlinear differential equation appears in various contexts such as the description of overdamped pendula, superconducting Josephson junctions, and the synchronized emission of light by fireflies.^{6,28}

For $0 \leq \omega_0 < \omega_c$ it has two fixed points characterized by $\dot{\phi} = 0$ (*i.e.* constant phase difference): One solution is a global attractor with $\phi = \arcsin(\omega_0/\omega_c)$, and the other one is unstable with $\phi = \pi - \arcsin(\omega_0/\omega_c)$. These two solutions correspond to the phase differences at which the torque due to friction equals the torque that is due to the field. At $\omega_0 = \omega_c$, *i.e.* at $\phi = \pi/2$, the two solutions form a saddle-node bifurcation and there are no fixed points for $\omega_0 > \omega_c$. At these high frequencies, the maximal torque that can be exerted by the field is insufficient to balance the frictional torque. The solution emerging after the bifurcation is a limit cycle with $\dot{\phi} > 0$.

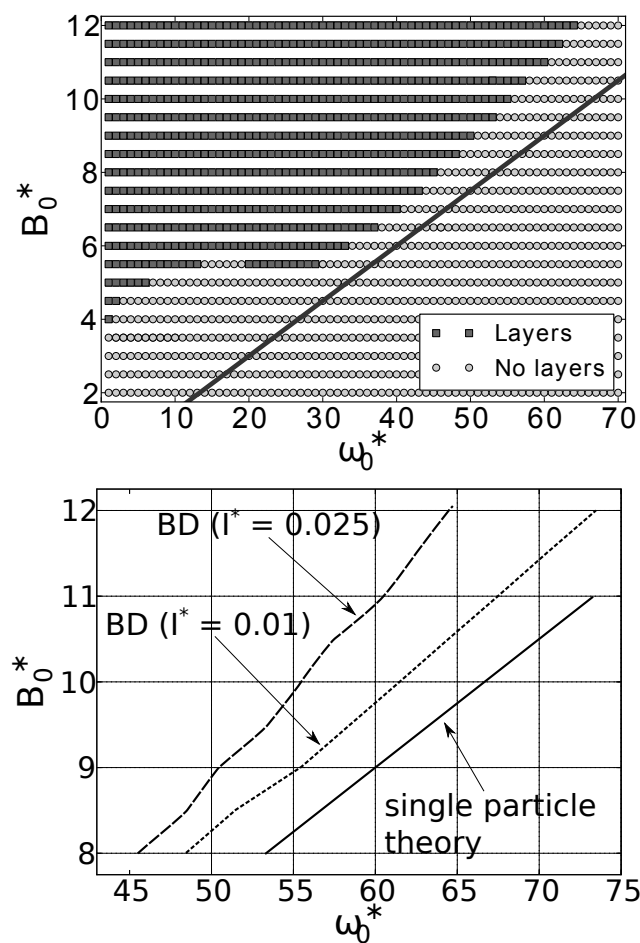


Fig. 10 (a) The solid line shows the critical frequencies $\omega_c = \mu B_0 / \xi_R$ that are predicted by the single-particle theory in the BD frequency-field strength diagram (see Fig. 4). (b) Influence of the moment of inertia on the end of layer formation (dashed line: $I^* = 0.025$, dotted line: $I^* = 0.01$). The solid line indicates the frequencies ω_c^* .

To which extent does the single-particle approach describe the true many-particle system of our BD simulations? In Fig. 10a, the frequencies ω_c (with $\gamma \equiv \xi_R$, see eqn (5)) are plotted

into the $\omega_0^* - B_0^*$ -state diagram (Fig. 4). At large frequencies ω_0^* and field strengths B_0^* , the straight line representing ω_c has a slope similar to that of the boundary of the layered regime. This supports the idea that it is the (rotational) friction which eventually yields a breakdown of the synchronous rotations, and thus, the layering. A further observation from Fig. 10a is that the true boundary frequencies (at given B_0^*) are somewhat smaller than ω_c . One seemingly obvious reason for these deviations is that the effective theory neglects any many-particle effects. Moreover, it does not take the Brownian random contributions into account that mimic the solvent “kicks” in eqn (5). Both these factors could introduce perturbations of the effective field that acts on a particle. Thereby the synchronized state could be destabilized already at frequencies $\omega < \omega_c$. However, as it turns out, the more significant reason for the premature stop of layering is that the BD equations of motion involve (rotational) inertial terms, which are neglected in our single-particle approach.

To check this point, we have performed additional BD simulations with a lower moment of inertia ($I^* = 0.01$). The resulting frequencies characterizing the boundary of the layered state are shown in Fig. 10b along with the original result ($I^* = 0.025$) and the line ω_c . Clearly, decreasing the moment of inertia moves the true boundary substantially closer to the single-particle result.

Finally, we note that the influence of the inertial (rotational) term can also be captured within our effective single particle theory. For $I \neq 0$, eqn (16) can be written as

$$\frac{d^2\phi}{d\tau'^2} + \nu \frac{d\phi}{d\tau'} = \frac{\omega_0}{\omega_c} - \sin\phi \quad (18)$$

with $\nu = \gamma/\sqrt{\mu B_0 I}$ and $\tau' = \sqrt{\mu B_0/I}t$. Similar to (16), this differential equation has a bifurcation at ω_c ,²⁸ which means that the location of the line ω_c in Fig. 10a remains unchanged.²⁸ As before, the only stable solution at driving frequencies that are larger than ω_c is a limit cycle. But additionally, for sufficiently small ν , it has a second bifurcation for some ω' with $\omega' < \omega_c$ as shown by Argentina *et al.* while investigating the transition between annihilation and preservation of colliding waves.²⁹ This second bifurcation introduces a regime in which the limit cycle can coexist with the stable rotation. From the perspective of a many-particle system, one may speculate that the presence of the second solution perturbs the rotation with constant phase difference (*i.e.*, $\dot{\phi} = 0$).

3.4 A density functional approach to layering in a perfectly synchronized system

We now consider systems at relatively low driving frequencies ($\omega_0^* \lesssim 30$), where, for sufficiently large field strengths B_0^* , the dipole vectors can follow the field in a perfectly synchronized fashion (see the discussion in the preceding sec-

tion). According to our “phase” diagram in Fig. 4, the field strength required to induce such synchronous and, at the same time, layered states, is about $B_0^* \approx 4 - 6$ for $\omega_0^* \lesssim 30$. The corresponding dipole-field coupling parameter $\mu B_0/k_B T = \mu^* B_0^*/T^* \approx 12$ is significantly larger than the dipole-dipole coupling parameter ($\lambda \approx 6.7$). Nevertheless, as seen in Figs. 3a and b as well as Fig. 5, increasing B_0^* from zero at low driving frequencies yields a rather slow increase of the order parameter ψ and the magnetization amplitude.

Given the apparent interconnectedness between the rotational dynamics of the individual dipoles and the layering of the particles, we ask in the present section whether synchronization leads *automatically* to layering. Indeed, even in a perfectly rotating system, one would expect that the spatial symmetry-breaking associated with layering yields a decrease of translational entropy and thus may be unfavorable.

To investigate this question we employ *equilibrium* density functional theory (DFT) for a system in which the dipole rotations are perfectly synchronized. Under such conditions the particles effectively interact via the time-averaged (inverted) dipolar potential given in eqn (12). By using this potential, the problem thus reduces to searching for an equilibrium *phase transition* in a system with effectively static interactions.

Our density functional approach is based on the perturbation expansion of the free energy originally proposed by Ramakrishnan and Yussouff in the context of fluid-solid transitions.³⁰ Up to second order in the density, the difference between the Helmholtz free energy of a volume V of a system with non-uniform density $\rho(\mathbf{r})$ and a reference system with homogeneous density ρ_0 is given by³¹

$$\begin{aligned} \frac{\Delta\mathcal{F}}{V} = & \frac{1}{\beta V} \int_V d^3r [\log(\Lambda^3 \rho(\mathbf{r})) - 1] \\ & - \frac{1}{\beta V} \int_V d^3r \rho_0 [\log(\lambda^3 \rho_0) - 1] \\ & - \frac{1}{2\beta V} \int_V d^3r_1 \int_3 d^3r_2 c(\mathbf{r}_1 - \mathbf{r}_2)|_{\rho_0} \Delta\rho(\mathbf{r}_1) \Delta\rho(\mathbf{r}_2). \end{aligned} \quad (19)$$

In eqn (19), $\Delta\rho(\mathbf{r}) = \rho(\mathbf{r}) - \rho_0$ with $\int_V d^3r \Delta\rho(\mathbf{r}) = 0$, Λ is the thermal wavelength, and $c(\mathbf{r})|_{\rho_0}$ is the direct correlation function of the homogeneous system.

Here we employ the random phase approximation (RPA) to calculate the direct correlation function.³² Assuming a hard sphere interaction in addition to the inverse dipolar potential U^{ID} (eqn (12)), the RPA amounts to setting

$$c(\mathbf{r}) = \begin{cases} c^{\text{PY}}(r), & r \leq \sigma \\ -\beta U^{\text{ID}}(\mathbf{r}), & r > \sigma, \end{cases} \quad (20)$$

where we used the Percus-Yevick direct correlation function, c^{PY} ,³² for the hard-sphere part. Note that within the RPA, the effects of the contributions of the long-ranged inverse dipolar interaction are treated in a mean-field fashion. To check

this point, we have also calculated $c(\mathbf{r})$ numerically by solving the mean-spherical (MSA) integral equations.³² However, the changes in the free energies were found to be marginal.

As a simple ansatz for the density profile in the layered state, we use

$$\rho(\mathbf{r}) = \rho(z) = \rho_0 + \tilde{\rho} \cos(kz). \quad (21)$$

Inserting this ansatz into eqn (19), we find

$$\frac{\Delta\mathcal{F}}{A} = \frac{1}{\beta} \int_0^{\lambda_L} dz \rho(z) \log\left(\frac{\rho(z)}{\rho_0}\right) - \lambda_L \frac{\tilde{\rho}^2}{4\beta} \tilde{c}(k), \quad (22)$$

where $\Delta\mathcal{F}$ is the free energy of the volume $A \cdot \lambda_L$, A is an area in the $x - y$ -direction and $\lambda_L = 2\pi/k$. Further, \tilde{c} is the Fourier transform of c and $\tilde{c}(k) \equiv \tilde{c}(k\mathbf{e}_z)$. In the RPA, we have

$$\tilde{c}(k) = 4\pi \left(\int_0^\sigma dr r^2 j_0(kr) c^{\text{PY}}(r) + \mu^2 \beta \frac{j_1(k\sigma)}{k\sigma} \right), \quad (23)$$

where j_n are spherical Bessel functions of order n . (For the treatment of the dipolar interactions in eqn (23), see Ref. 33) We now use eqn (22) to search for a phase transition between the homogeneous and the layered state. In principle, this search requires a minimization of $\Delta\mathcal{F}/A$ with respect to both the parameters $\tilde{\rho}$ and k that characterize the inhomogeneity of the system (see eqn (21)). It turns out, however, that $\Delta\mathcal{F}/A$ becomes minimal with respect to k for $k \rightarrow 0$, which corresponds to an *infinite* distance between the layers. Clearly, this is not compatible with the implicit assumption of a finite wavelength. Therefore we have fixed the parameter $k = 2\pi/\lambda_L$ to physically reasonable values, *i.e.* to values suggested by our BD simulations. At $\rho_0^* = 0.1$, we find an average layer distance of approximately 7.2σ (see below). This leaves the coefficient $\tilde{\rho}$ as the only minimization parameter. Results for the function $\Delta\mathcal{F}(\tilde{\rho})/(A\lambda_L)$ with fixed distance $\lambda_L = 7.2\sigma$ between the layers at various values of the parameter μ^* are plotted in Fig. 11a.

The different curves in Fig. 11a reveal a behavior typical of a second-order phase transition. For $\mu^* \lesssim 2.27$, the free energy has only one minimum at $\tilde{\rho} = 0$ corresponding to an homogeneous state. This changes at $\mu_c^* \approx 2.27$: For larger values of μ^* , the solution at $\tilde{\rho} = 0$ represents a maximum, and the only minimum occurs for $\tilde{\rho} > 0$. The corresponding negative values of $\Delta\mathcal{F}/A$ indicate that it is indeed the layered state which is now globally stable.

We have repeated the DFT calculations for a number of densities in the range $0.01 \leq \rho_0^* \leq 0.4$. To find reasonable values for the corresponding wavelengths λ_L in the layered state, we ran BD simulations at fixed dipole moment $\mu^* = 3.4$, frequency $\omega_0^* = 8$, and field strength $B_0^* = 50$. With this choice of the parameters, the particles are almost perfectly aligned, justifying the key assumption of our DFT approach. Fitting

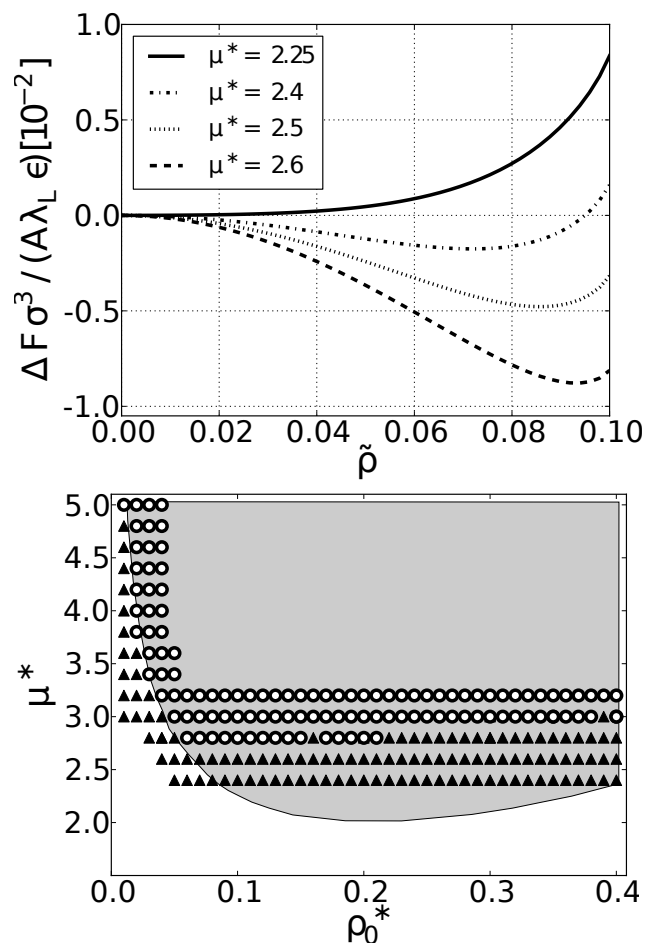


Fig. 11 (a) Free energy difference between a layered and a homogeneous state as a function of the coefficient $\tilde{\rho}$ (see eqn (21)) at different values of the parameter μ^* . The case $\tilde{\rho} = 0$ corresponds to the homogeneous solution. The overall density is set to $\rho_0^* = 0.1$. (b) Equilibrium phase diagram of a perfectly synchronized system. The gray area indicates the stability range of the layered state according to our DFT calculations. Also shown are BD results (at $\omega_0^* = 8$, $B_0^* = 50$) with the open circles (solid triangles) representing layered (non-layered) states.

the resulting distances as functions of ρ_0 , we found the approximate relation $d/\sigma \approx 1.05\rho_0^{*-0.84}$, which was then used as an input in the DFT (*i.e.*, $\lambda_L = d$).

The resulting phase diagram in the $\rho_0^* - \mu^*$ -plane is plotted in Fig. 11b. It is seen that the DFT predicts a layering transition for all but the smallest densities ($\rho_0^* \gtrsim 0.01$) in the shown parameter range, with the actual values of μ_c^* varying substantially with ρ_0^* . Indeed, the lowest threshold is found at $\rho_0^* \approx 0.2$. Also shown in Fig. 11b are BD results for the appearance of layers in nearly perfectly synchronized systems ($\omega_0^* = 8$, $B_0^* = 50$) at various values of μ^* . As in Sec. 3.2, the presence of layers was detected on the basis of the order pa-

parameter defined in eqn (13), yet with a slightly different definition of the cutoff radius entering the order parameter ($r_0 = d$). Comparing BD and DFT, it is seen that the DFT predicts the true phase boundary in perfectly synchronized systems in a qualitatively correct manner (including the strong increase of μ_c^* upon $\rho_0^* \rightarrow 0$). Moreover, the DFT results are also quite reasonable from a quantitative point of view.

From a physical perspective, clearly the most important conclusion is that even in a perfectly synchronized system, a sufficient decrease of interaction energy stemming from the time-averaged dipolar potential is required to overcome the entropy cost due to layering.

Finally, we briefly discuss our DFT results in the light of a recent Monte Carlo study by Smallenburg and Dijkstra,²¹ who obtained full equilibrium phase diagrams of systems interacting with inverted dipolar interactions. To model the short-range part of the interaction, Smallenburg and Dijkstra used either just hard spheres or hard spheres with an additional Yukawa repulsion.²¹ In the first case, layer-like structures were only observed in the gas-liquid coexistence region. On the contrary, the Yukawa system exhibits a stable layered phase with fluid-like in-plane structure. Comparing these latter results to our DFT predictions, we find that the predicted strength of the inverted dipolar interactions required for layer formation is indeed comparable. On the other hand, we find the onset of layer formation at much lower densities. Apart from the obvious approximations in our theory, we also attribute these deviations to the fact that the repulsive Yukawa interaction used in Ref. 21 is much stronger than our soft sphere one.

4 Conclusions

In this study we have combined BD computer simulations, an effective single-particle theory, and an (equilibrium) density functional approach to explore the dynamic behavior of systems of dipolar particles in planar rotating fields.

One main result from our BD simulations is a non-equilibrium “phase” diagram identifying the domain of layered states in the ω_0 - B_0 plane (at constant particle density and dipolar coupling strength). At low driving frequencies, the change from unlayered to layered (and fully synchronized) structures occurring upon increase of B_0 is related to a quasi-equilibrium phase transition, *i.e.* a many-particle phenomenon. The transition is induced by the competition between the time-averaged, inverted dipolar interactions favoring in-plane configurations and the loss of translational entropy accompanying the one-dimensional translational order. While this competition also occurs for systems of polarizable or superparamagnetic particles, the additional complication in the present system of permanent dipoles is that the field first needs to overcome the dipolar fluctuations. Though we have

neglected this issue in our DFT approach, we would expect that the fluctuations just shift the transition predicted by the DFT towards larger field strength.

Completely different behavior is found at high frequencies and field strengths. Under these conditions, the picture of synchronously rotating dipoles (with constant phase difference relative to the field) breaks down. Instead, one observes a mixture of rotating and counter-rotating or resting particles, as our analysis of various angle distributions reveals. The desynchronization induces, at the same time, a breakdown of the translational, layered structure. Despite this complex many-particle behavior, we have shown that the boundary can be well described in terms of the critical frequency $\omega_c(B_0)$ that arises from a bifurcation in an effective *single-particle* approach for the rotational motion in a viscous medium. This indicates that the appearance of the high-frequency boundary is essentially a friction-induced effect.

A similar frequency-induced desynchronization effect has recently been discussed by Härtel *et al.*,²³ who investigated a system of interacting elongated particles in a rotating electric field via dynamic density functional theory. Assuming a constant number density, the important dynamic variable within the density functional approach is the orientational distribution as function of time. At low and very high frequencies, the distribution behaves similar to our distribution f in that there is either a single peak (reflecting synchronized motion with a constant phase difference) or no peak at all. In the transition regime, however, Härtel *et al.* detected various new dynamic states characterized by time-dependent oscillations and splitting of the peak in the distribution as well as an overtaking by the driving field. In the present study we did not observe such states, not even when looking at the time-dependence of our orientational distributions (or the magnetization). It remains to be investigated whether these qualitative differences in the rotational motion of anisotropic many-particles systems are just due to differences in the specific model system, or due to the fact that our results are based on a microscopic approach rather than on the density field approach used in Ref. 23. Indeed, the relation between the microscopic and mesoscopic dynamics in driven systems is an issue also discussed in other, related contexts, such as the shear-induced dynamics of nanorods.³⁴

Finally, it is worth to briefly comment on the relevance of our dimensionless model parameters in the context of real systems. The equilibrium parameters considered here (density $\rho^* = 0.1$, dipolar coupling strength $\lambda \approx 6.7$) correspond to those of a strongly coupled ferrofluid exhibiting chain formation.¹⁴ Regarding the driving field, however, most of our dimensionless frequencies ω_0^* are probably beyond the currently accessible range. In many experiments involving rotating fields, the size of the (typically superparamagnetic) particles considered is about $1 \mu\text{m}$.^{4,11} A driving frequency of

$\omega_0^* = 10$ (which is well within the layered domain) then corresponds to an actual frequency of about 10 kHz if we assume room temperature ($T = 293$ K) and a mass density of 5 g/cm^3 . This is 1-2 orders of magnitudes larger than the frequencies used in the literature.^{4,11} Ferrocolloidal particles, which have permanent dipoles (such as the ones considered here), are often much smaller with sizes of about 10 nm. In that case, $\omega_0^* = 10$ corresponds to a driving frequency of about 1 GHz.

These considerations suggest that realistic driven systems will be fully synchronized and layered according to our “phase” diagram in Fig. 4. We note, however, that the actual location of the desynchronization line encountered upon increasing ω_0^* depends on the friction constant used in our BD simulations; *i.e.*, increasing the friction constant shifts the line towards lower frequencies (consistent with the single-particle theory). Moreover, we have neglected in our study the many-particle character of the hydrodynamic interactions induced by the solvent. We would expect these interactions to effectively increase the friction and thus shift the boundary towards even lower frequencies. Clearly, it would be very interesting to actually incorporate such interactions by using refined simulation methods such as, *e.g.*, stochastic rotation dynamics.³⁵ Hydrodynamic interactions may also be relevant to better explore phenomena such as chain-to-cluster transitions that have been revealed by recent studies.⁴ These issues, as well as the dynamic behavior in even more complex field geometries, will be the subject of future studies.

5 Acknowledgements

We gratefully acknowledge financial support from the DFG within the research training group RTG 1558 *Nonequilibrium Collective Dynamics in Condensed Matter and Biological Systems*, project B1.

References

- 1 P. Tierno, J. Claret, F. Sagués and A. Cēbers, *Phys. Rev. E*, 2009, **79**, 021501.
- 2 N. Coq, S. Ngo, O. du Roure, M. Fermigier and D. Bartolo, *Phys. Rev. E*, 2010, **82**, 041503.
- 3 P. Dhar, C. D. Swayne, T. M. Fischer, T. Kline and S. Ayusman, *Nano Lett.*, 2007, **7**, 1010.
- 4 N. Casic, S. Schreiber, P. Tierno, W. Zimmermann and T. M. Fischer, *EPL*, 2010, **90**, 58001.
- 5 R. Dreyfus, J. Baudry, M. Roper, M. Fermigier, H. Stone and J. Bibette, *Nature*, 2005, **437**, 862.
- 6 W. A. Shelton, K. D. Bonin and W. T. G., *Phys. Rev. E*, 2005, **71**, 036204.
- 7 M. E. Leunissen, H. R. Vutukuri and A. v. Blaaderen, *Adv. Mater.*, 2009, **21**, 3116.
- 8 J. F. Douglas, *Nature*, 2010, **463**, 302.
- 9 J. E. Martin, R. A. Anderson and C. P. Tigges, *J. Chem. Phys.*, 1998, **108**, 7887.
- 10 J. E. Martin, R. A. Anderson and C. P. Tigges, *J. Chem. Phys.*, 1999, **110**, 4854.
- 11 N. Elsner, C. P. Royall, B. Vincent and D. R. E. Snoswell, *J. Chem. Phys.*, 2009, **130**, 154901.
- 12 T. C. Halsey, R. A. Anderson and J. E. Martin, *Int. J. Mod. Phys. B*, 1996, **10**, 3019.
- 13 J. Philip, P. D. Shima and B. Raj, *Appl. Phys. Lett.*, 2007, **91**, 203108.
- 14 K. Butter, P. H. H. Bomans, P. M. Frederik, G. J. Vroege and A. P. Philipse, *Nature Mater.*, 2003, **2**, 88.
- 15 J. Jordanovic, S. Jäger and S. H. L. Klapp, *Phys. Rev. Lett.*, 2011, **106**, 038301.
- 16 U. Dassanayake, S. Fraden and A. van Blaaderen, *J. Chem. Phys.*, 2000, **112**, 3851.
- 17 A.-P. Hynninen and M. Dijkstra, *Phys. Rev. Lett.*, 2005, **94**, 138303.
- 18 J. E. Martin, E. Venturini, G. Gulley and J. Williamson, *Phys. Rev. E*, 2004, **68**, 021508.
- 19 J. E. Martin, R. A. Anderson and J. Williamson, *J. Chem. Phys.*, 2003, **118**, 1557.
- 20 N. Ostermann, I. Poberaj, J. Dobnikar, D. Frenkel, P. Ziherl and D. Babić, *Phys. Rev. Lett.*, 2009, **103**, 228301.
- 21 F. Smallenburg and M. Dijkstra, *J. Chem. Phys.*, 2010, **132**, 204508.
- 22 V. V. Murashov and G. N. Patey, *J. Chem. Phys.*, 2000, **112**, 9828.
- 23 A. Härtel, R. Blaak and H. Löwen, *Phys. Rev. E*, 2010, **81**, 051703.
- 24 S. H. Klapp and M. Schoen, *Reviews in Computational Chemistry*, Wiley, 2007, vol. 24.
- 25 M. P. Allen and D. J. Tildesley, *Computer Simulations of Liquids*, Oxford University Press, 1986.
- 26 J. J. Weis and D. Levesque, *Phys. Rev. Lett.*, 1993, **71**, 2729.
- 27 J. Delhommelle, J. Petracic and D. J. Evans, *J. Chem. Phys.*, 2004, **120**, 6117.
- 28 S. H. Strogatz, *Nonlinear Dynamics and Chaos*, Westview Press, 2000.
- 29 M. Argentina, P. Couillet and L. Mahadevan, *Phys. Rev. Lett.*, 1997, **79**, 2803.
- 30 T. V. Ramakrishnan and M. Yussouf, *Phys. Rev. B*, 1979, **19**, 2775.
- 31 A. D. J. Haymet and D. W. Oxtoby, *J. Chem. Phys.*, 1981, **74**, 2559.
- 32 J.-P. Hansen and J. R. McDonald, *Theory of simple Liquids*, Academic Press, 2006.
- 33 D. Wei, G. N. Patey and A. Perera, *Phys. Rev. E*, 1993, **47**, 506.
- 34 Y.-K. Tao, W. K. den Otter and W. J. Briels, *EPL (Europhysics Letters)*, 2009, **86**, 56005.
- 35 A. Malevanets and R. Kapral, *J. Chem. Phys.*, 1999, **110**, 8605.